

Article

Experimental and Theoretical Studies of the Corrosion Inhibition Performance of a Quaternary Phosphonium-Based Ionic Liquid for Mild Steel in HCl Medium

Lei Guo ^{1,2,*}, Yue Huang ^{3,†}, Yundong Wu ¹, Wei Shi ^{3,*}, Faheem Abbas ⁴, Yuanhua Lin ², Riadh Marzouki ^{5,6} and Xingwen Zheng ⁷

¹ School of Materials and Chemical Engineering, Tongren University, Tongren 554300, China

² School of Oil and Natural Gas Engineering, Southwest Petroleum University, Chengdu 610500, China

³ College of Materials and Metallurgy, Guizhou University, Guiyang 550025, China

⁴ Department of Chemistry, Tsinghua University, Beijing 100084, China

⁵ Chemistry Department, College of Science, King Khalid University, Abha 61413, Saudi Arabia

⁶ Chemistry Department, Faculty of Sciences, University of Sfax, 1171, Sfax 3000, Tunisia

⁷ School of Chemical and Environmental Engineering, Sichuan University of Science and Engineering, Zigong 643099, China

* Correspondence: chygl@gztrc.edu.cn (L.G.); wshi@gzu.edu.cn (W.S.)

† These authors contributed equally to this work.

Abstract: The corrosion inhibition performance of a quaternary phosphonium-based ionic liquid, i.e., hexadecyltriphenylphosphonium bromide (HPP), on mild steel in 1 M HCl solution was investigated by electrochemical impedance spectroscopy (EIS) and potentiodynamic polarization (PDP) methods. The surface characterization of mild steel was examined by scanning electron microscopy with energy-dispersive X-ray spectroscopy (SEM-EDS). The results revealed that the inhibition efficiency increases with its increasing concentration, and it can reach up to 99.1% at the concentration of 0.07 mM HPP. PDP data showed that the adsorption of HPP conformed to Langmuir adsorption, which served as a mixed-type inhibitor, involving chemisorption and physisorption. SEM analysis confirmed the formation of barrier film on the metal surface, inhibiting the acid attack. Moreover, density functional theory (DFT) calculations and molecular dynamics (MD) simulations were conducted to elucidate the adsorption mechanism of inhibitor molecules on the mild steel surface. A match between the experimental and theoretical findings was evidenced.

Keywords: mild steel; corrosion inhibition; hexadecyltriphenylphosphonium bromide; molecular simulation; electrochemistry



Citation: Guo, L.; Huang, Y.; Wu, Y.; Shi, W.; Abbas, F.; Lin, Y.; Marzouki, R.; Zheng, X. Experimental and Theoretical Studies of the Corrosion Inhibition Performance of a Quaternary Phosphonium-Based Ionic Liquid for Mild Steel in HCl Medium. *Sustainability* **2023**, *15*, 3103. <https://doi.org/10.3390/su15043103>

Academic Editor: Agostina Chiavola

Received: 21 December 2022

Revised: 22 January 2023

Accepted: 6 February 2023

Published: 8 February 2023



Copyright: © 2023 by the authors. Licensee MDPI, Basel, Switzerland. This article is an open access article distributed under the terms and conditions of the Creative Commons Attribution (CC BY) license (<https://creativecommons.org/licenses/by/4.0/>).

1. Introduction

Mild steel is widely applied in the construction, food processing, gas storage tanks, vehicles, bridge fields on account of its excellent mechanical strength, ductility, easy production, and low cost [1,2]. However, the structure and functionality of mild steel will be altered by corrosion. In extreme circumstances, they will cause the material's surface to crack. This kind of cracking can occasionally result in significant financial losses and casualties [3]. Therefore, it is urgent to prevent mild steel from corrosion. In recent years, various anti-corrosion strategies emerged, mainly including adding corrosion inhibitors, coating isolation, alloying, metal surface modification [4,5]. Compared with other strategies, the application and addition of inhibitor has become the simplest and economical approach [6–8]. Inhibitors are chemicals that adhere to the surface of metal to produce a barrier that prevents corrosion on materials [9–11]. Without affecting the original performance of metal materials, adding a little amount of corrosion inhibitor can dramatically lower the rate of corrosion of materials in the environmental medium.

Seeking a corrosion inhibitor that can be widely used in industry is urgent, especially in high-risk fields such as the metal pickling and acidization treatment. Recently, ionic liquids, particularly the four varieties depicted in Figure 1, have become increasingly popular due to their distinctive properties, which include low toxicity, high polarity, low cost, non-flammability, low vapor pressure, excellent solubility, and thermal stability [12–14]. The researchers discovered that many kinds of ionic liquids can effectively suppress metal corrosion. For example, Ech-chihbi and co-workers investigated the anti-corrosion properties of three imidazolium-based ionic liquids on mild steel in 1 M HCl solution [15]. According to the research, these synthesized ionic liquids exhibited excellent corrosion inhibiting property >90%. According to Liu et al., three imidazole ionic liquids can reduce the corrosion rate of N80 steel at high temperatures and high acid concentrations [16]. They verified that the longer the alkyl chain of the three investigated corrosion inhibitors, the more effective they were at inhibiting corrosion. Furthermore, Zheng and colleagues reported a new benzimidazole derivative, i.e., 1-butyl-3-methyl-1H-benzimidazolium iodide (BMBIMI), as inhibitor for mild steel in 0.5 M H₂SO₄ solution, and they confirmed that their own iodide ion and BMBIMI cations have a synergistic inhibitory effect, which enhances the overall corrosion inhibition performance [17]. On this basis, we introduced a newly generated terminology, viz., *homologous self-synergistic inhibition effect*, for ionic liquid-based corrosion inhibitors.

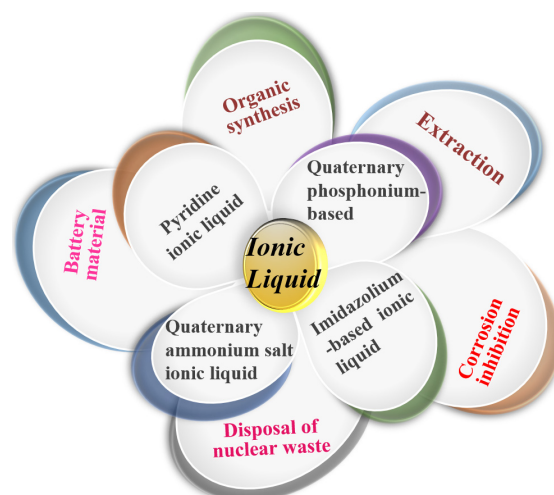


Figure 1. Classification and applications of ionic liquids.

Regrettably, neither the inhibition mechanism nor the conformational relationship between inhibition efficacy and molecular structure are fully understood, which still needs further experimental confirmation. Therefore, as a phosphorus-based ionic liquid, hexadecyltriphenylphosphonium bromide (HPP) was selected as a potential corrosion inhibitor for mild steel in HCl solution in this study. Electrochemical experiments were adopted to assess its inhibition performance. The present work offers a workable strategy for developing novel sustainable corrosion inhibitors and aids in understanding the anticorrosive mechanism of related ionic liquid-based inhibitors.

2. Experimental

2.1. Materials and Reagents

Mild steel sheets (purchased from Shanghai Ronghan Industrial Co., Shanghai, China) were used and the chemical composition is as follows: 0.04% S, 0.04% P, 0.13% Mn, 0.18% Si, 0.17% C, and Fe for balance. HPP (purity, 98%) was supplied by Shanghai Aladdin Industrial Corporation (Shanghai, China). HCl (purity, 37%) was purchased from Sinopharm Chemical Reagent. Concentrated HCl and ultrapure water were used to prepare corrosive medium (1 M HCl). HPP with concentrations of 0.01, 0.03, 0.05, 0.07, and 0.09 mM were selected. All chemicals and solvents were used as received without any further purification.

2.2. Electrochemical Measurements

Electrochemical experiments were implemented using a typical three-electrode system by CHI660E electrochemical workstation with its own software, which was purchased from Shanghai Chenhua Instrument Co., Ltd. It consists of a platinum sheet, a saturated calomel electrode (SCE), and mild steel, which were employed as the counter, reference, and working electrodes, respectively. A block of mild steel was made that was 1 cm × 1 cm × 1 cm, then sealed with epoxy resin (exposed area of 1 cm²), which as the working electrode. Before each experiment, the steel sample was polished and with polishing paper of different roughness (120 #, 240 #, 400 #, 600 #, 800 #, 1000 #), cleaned in the distilled water, then degreased with ethanol and dried at room temperature. Firstly, the working electrode's open circuit potential (E_{OC}) was tested. Then, testing of the electrochemical impedance curve continued with a consistent open circuit value using the same working electrode. The impedance test applied a frequency range of 100~0.1 Hz with 10 mV amplitude and used ZsimpWin software to analyze the obtained impedance data. Finally, potentiodynamic polarization measurement was conducted scanning within −250 mV to 250 mV potential range at 0.02 mV/s versus E_{OC} . In order to reduce experimental error, all tests were conducted three times.

2.3. Surface Analysis

The surface morphology and elemental composition of mild steel immersed in inhibited and uninhibited HCl solution for 6 h at 298 K was tested via SEM-EDS (JEOL-JSM-7800F) operated at 20 kV accelerating voltage. SEM examined the morphological changes, EDS, and elemental mappings analysis furnished the composition of the steel surface after dipping into test solutions with and without HPP. To guarantee the accuracy and reliability, all samples were washed with absolute ethanol and ultrapure water, and then dried in a vacuum oven.

2.4. UV-Visible Analysis of the Solution

The UV-vis curves of mild steel after soaking in blank solution and in solution with optimal concentration of HPP inhibitor for 6 h were studied. After that, the resultant solution was examined using a TU-1901 spectrophotometer with a quartz tube. Specifically, this technique was intended to determine whether the inhibitor and Fe forms a complex.

2.5. Computational Methodology

2.5.1. DFT Calculations

To investigate the electronic structures of HPP inhibitor, quantum chemistry calculations were adopted by DFT with the GGA-BLYP exchange correlation function using the Dmol³ module of Material Studio (MS) software (BIOVIA Company, San Diego, CA, USA) [18]. In addition, it is emphasized that a double numeric quality and polarization (DNP) basis set was used with the COSMO implicit solvent model (dielectric constant of water: 78.54), where the reliability of this level of theory in studying organics has been confirmed [19,20]. Vibration analysis was conducted in the test to make the structure reach the minimum point of potential energy surface after optimization. The convergence thresholds for energy, displacement, and force were 1×10^{-5} Ha, 5×10^{-3} Å, 2×10^{-3} Ha/Å, respectively.

2.5.2. Molecular Dynamics Simulation

The Forcite module of the MS software was used to explore the adsorption mechanism of HPP on the surface of mild steel [21]. Fe(110) crystal slab was selected as a representative of the steel surface because of its proven most favorable configuration based on the combined factors such as facet area, surface energy, and coordination numbers [22]. The geometry of the cleaved surface was optimized using COMPASSII (condensed phase optimized molecular potentials for atomistic simulation studies II) force field and subse-

quently enlarged to a 10×10 supercell. The nonbond interaction energy of COMPASSII is calculated by the following formula, which is an ab initio force field [23]:

$$E_{\text{nonbond}} = \sum_{ij} \varepsilon_{ij} \left[2 \left(\frac{r_{ij}^0}{r_{ij}} \right)^9 - 3 \left(\frac{r_{ij}^0}{r_{ij}} \right)^6 \right] + \sum_{ij} \frac{q_i q_j}{r_{ij}} \quad (1)$$

where ε_{ij} is the energy parameter between atoms i and j , r_{ij}^0 means the dimension parameter, r_{ij} represents the distance between particles i and j , and q_i and q_j are the charges of i and j atoms, respectively. The Andersen thermostat was used to control the system temperature of 298 K, and a simulation box with periodic boundary conditions with dimensions of $24.8 \times 24.8 \times 39.1 \text{ \AA}^3$ was employed. The step size was set to 1 fs, and the total simulation time was 1000 ps.

3. Results and Discussion

3.1. Open Circuit Potential and PDP Analysis

The variation in the E_{OC} values of the mild steel electrode with immersion time is analyzed. As depicted in Figure 2a, in comparison to the E_{OC} of the sample submerged in the corrosion solution without HPP, Figure 2a shows a consistent declining trend when HPP inhibitor is introduced to the corrosion solution. This event demonstrates that the formation of a stable protective film on the metal surface following the addition of HPP inhibitor.

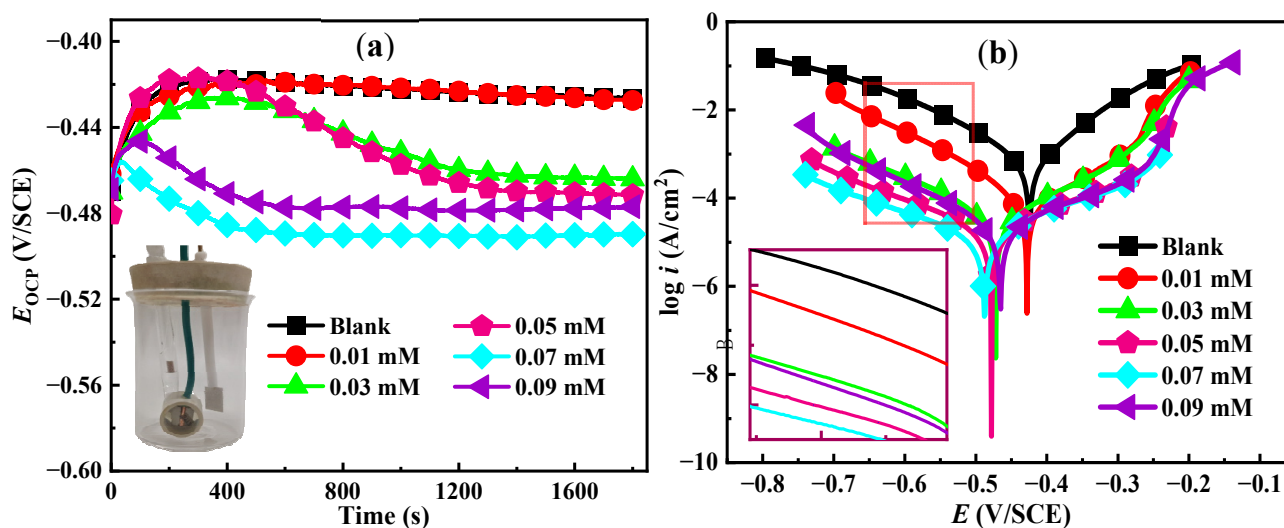


Figure 2. (a) Open circuit potential and (b) polarization curves of mild steel in 1 M HCl solution with and without HPP inhibitor.

The PDP curve is one of the most frequently used techniques to explore the corrosion kinetics. The potentiodynamic polarization curves of mild steel electrode in 1 M HCl solution containing different concentrations of HPP inhibitor were shown in Figure 2b. As can be observed, the addition of HPP has no discernible impact on the cathode and anode branch shapes of the polarization curve, indicating that the investigated inhibitor does not alter the reaction mechanism of mild steel in 1 M HCl solution [24]. It is generally recognized that the inhibitor molecules mainly inhibit the corrosion process by preventing mild steel from coming into direct contact with the corrosive liquid. Compared with the blank solution, the Tafel curves after adding HPP inhibitor moved to the direction of low current density. The polarization parameters including corrosion current density (i_{corr}), cathode Tafel slope (β_c), anode Tafel slope (β_a), and corrosion potential (E_{corr}) were collected via the Tafel extrapolation method [25]. The inhibition efficiency (η_{PDP}) is measured by the following equation [26]:

$$\eta_{\text{PDP}}\% = \frac{i_{\text{corr},0} - i_{\text{corr}}}{i_{\text{corr},0}} \times 100 \quad (2)$$

where $i_{\text{corr},0}$ and i_{corr} stand for the corrosion current densities without and with the HPP inhibitor, respectively.

As obtained in Table 1, the corrosion potential of the blank condition was -0.426 V, which gradually changed to -0.489 V with the addition of HPP, and the potential change was significantly less than 85 mV. The slopes of anodic and cathodic Tafel lines (β_a and β_c) were lightly varied with the increasing of HPP concentration. This indicates that HPP is a mixed-type inhibitor, suppressing both anodic dissolution of iron and cathodic evaluation of hydrogen gas [27,28]. As can be seen, the inhibition rate at 0.09 mM was lower than 0.07 mM, indicating that 0.07 mM was the optimal inhibition concentration of HPP. The molecular concentration will achieve saturation at concentrations greater than 0.07 mM, generating competitive adsorption that will accelerate the corrosion of mild steel. We can see that when HPP concentration was 0.07 mM, the corrosion current density decreased to $15.79 \mu\text{A}/\text{cm}^2$, and the η_{PDP} value was up to 97.6%.

Table 1. Tafel polarization results of mild steel in 1 M HCl solution with different HPP concentrations.

C (mM)	E_{corr} (V/SCE)	i_{corr} ($\mu\text{A}/\text{cm}^2$)	β_c (mV/dec $^{-1}$)	β_a (mV/dec $^{-1}$)	η_{PDP} (%)
Blank	−0.426	669.2	−115	82	/
0.01	−0.427	77.39	−105	104	88.4
0.03	−0.464	38.63	−136	134	94.2
0.05	−0.472	21.41	−161	165	96.8
0.07	−0.489	15.79	−176	155	97.6
0.09	−0.477	26.37	−129	177	96.1

3.2. EIS Measurement

The impedance technique has been validated as an effective way for evaluating the performance of inhibitors. Herein, in order to investigate the corrosion of mild steel in 1 M HCl in the absence and presence of varying amounts of HPP, EIS measurements were conducted. The Nyquist and Bode plots were obtained and are presented in Figure 3. As depicted in Figure 3a, all the Nyquist curves exhibited similar shape behavior in the inhibited and uninhibited system. Nyquist plots all maintained a consistent shape for all concentrations and show as a single oblate capacitive loop, indicating that the corrosion inhibiting effect in 1 M HCl is controlled by the charge transfer mechanism [29]. The unique depressed capacitive loop results from the influence of frequency dispersive impacts, which can be caused by the electrode surface's roughness and inhomogeneity [30,31]. Bode diagrams in Figure 3b,c show a one-time constant in all HPP concentrations, indicating that charge transfer is the only relaxation process. Based on the Bode diagram for phase angle vs. $\log f$ the phase angle curves were significantly widened and significantly increased with increasing inhibitor concentration at 0.01–0.07 mM.

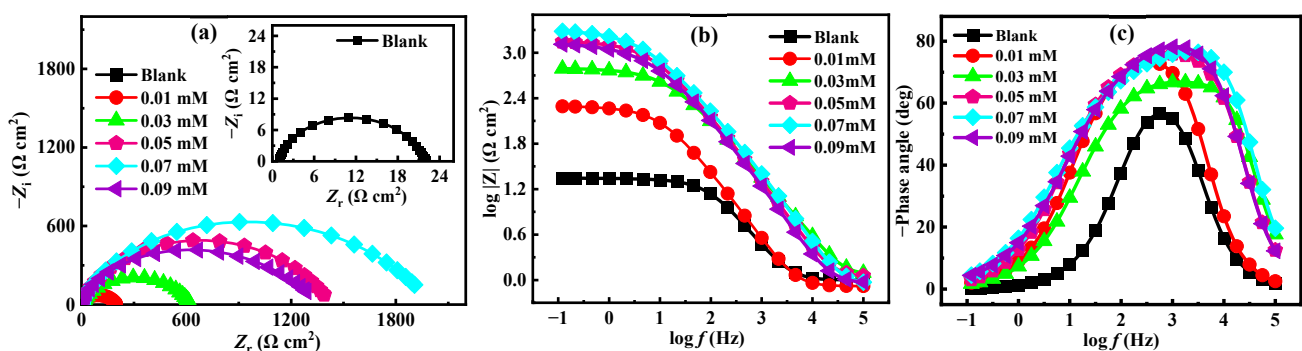


Figure 3. (a) Nyquist, (b) Bode modulus, and (c) Bode phase curves for mild steel in 1 M HCl solution without and with different concentrations of HPP inhibitor.

EIS data was further analyzed by fitting the equivalent circuit model shown in Figure 4. In the equivalent circuit diagram, R_s , R_f , R_{ct} , CPE_f , and CPE_{dl} represent solution resistance, corrosion product resistance, charge transfer resistance, constant phase angle element, and constant phase angle element of double-layer capacitance, respectively. The impedance function of CPE is described by the following equation [32,33]:

$$Z_{CPE} = Y_0^{-1}(j\omega)^{-n} \quad (3)$$

where Y_0 denotes the proportional factor, ω means the angular frequency, j stands for the imaginary unit, n represents a measure of non-uniform current distribution due to surface heterogeneity and its value lies between 0 and 1. When $n = 0$, CPE behaves as resistor; an ideal capacitor when $n = 1$ [34]. The inhibition efficiency (η_{EIS}) and double-layer capacitance (C_{dl}) were obtained from the following formula [35,36]:

$$\eta_{EIS}\% = \frac{R_{ct} - R_{ct}^0}{R_{ct}^0} \times 100 \quad (4)$$

$$C_{dl} = Y_0 \left(R_p^{1-n} \right)^{\frac{1}{n}} \quad (5)$$

where R_{ct}^0 and R_{ct} are the charge transfer resistance without HPP inhibitor and with HPP inhibitor, respectively. f_{max} refers to the maximum frequency at which the imaginary part of the impedance has a maximum value. The fitting degree between experimental data and the simulated results obtained by the proposed equivalent circuit was evaluated by the chi-square (χ^2) parameter, which is defined as [37]:

$$\chi^2 = \sum_{i=1}^n \left[\frac{\left(Z'_i(\omega_i, \vec{p}) - a_i \right)^2}{a_i^2 + b_i^2} + \frac{\left(Z''_i(\omega_i, \vec{p}) - b_i \right)^2}{a_i^2 + b_i^2} \right] \quad (6)$$

wherein, ω_i , a_i , b_i are experimental data points, \vec{p} is a factor connected with the proposed model, Z'_i and Z''_i are expected data points. The results incorporated in Table 2 show that the values χ^2 are of the order of 10^{-3} , indicating the accuracy of the equivalent circuit model.

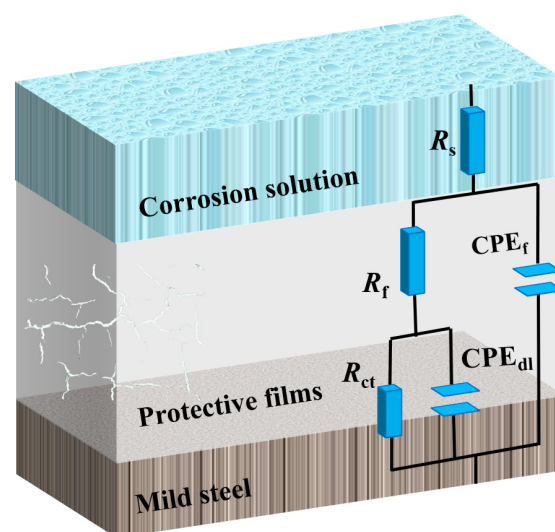


Figure 4. Equivalent circuit model for EIS fitting.

Table 2. Corrosion data of mild steel in HCl solution with and without HPP inhibitor.

C (mM)	R_s ($\Omega \text{ cm}^2$)	CPE _f		C_f ($\mu\text{F cm}^{-2}$)	R_f ($\Omega \text{ cm}^2$)	CPE _{d1}		C_{d1} ($\mu\text{F cm}^{-2}$)	R_{ct} ($\Omega \text{ cm}^2$)	χ^2 (10^{-3})	θ	η_{EIS} (%)
		Y_0 ($10^{-5} S_s^n \text{ cm}^{-2}$)	n_1			Y_0 ($10^{-5} S_s^n \text{ cm}^{-2}$)	n_2					
Blank	1.003	5.177	1.000	51.7	3.92	415.60	0.686	1241.0	17.1	8.22	/	/
0.01	0.832	4.336	1.000	43.3	13.90	24.74	0.644	45.0	185.2	2.17	0.907	90.7
0.03	1.171	42.20	1.000	422.0	12.07	6.39	0.689	14.8	612.6	2.88	0.972	97.2
0.05	1.106	64.20	0.999	639.2	19.50	4.82	0.664	12.4	1412.0	5.43	0.988	98.8
0.07	0.877	50.59	1.000	505.9	25.56	5.44	0.633	15.0	1986.0	8.10	0.991	99.1
0.09	0.919	78.92	1.000	789.2	17.24	8.19	0.582	16.6	1351.0	9.61	0.987	98.7

As shown in Table 2, the R_{ct} is $17.1 \Omega \text{ cm}^2$ for the blank condition. However, after the addition of HPP inhibitor, the values of R_{ct} increased gradually. When the inhibitor concentration reached 0.07 mM, the value of R_{ct} was changed to $1986.0 \Omega \text{ cm}^2$, and the corresponding inhibition efficiency was as high as 99.1%. However, we also recognize that the value of C_{d1} decreased compared with blank solution. This phenomenon can be explained by the Helmholtz model [38,39]:

$$C_{d1} = \frac{\epsilon \times \epsilon^0}{d} S \quad (7)$$

where ϵ and ϵ^0 are the local dielectric constant and the permittivity of vacuum, respectively; S refers to the surface area of working electrode; and d represents the thickness of the protective layer. The inhibitive adsorption was occurred at the steel/solution interface, which hindered the direct contact between metal and corrosive solution, thus reducing the exposed surface area of electrode and/or increasing the thickness of double electrode layer, and finally reducing the value of C_{d1} [40].

3.3. Adsorption Isotherm

The crucial adsorption information of HPP inhibitor on mild steel surface was discussed by adsorption isotherms. The isotherm was determined using the correlation coefficient (R^2) that best matches the acquired investigation data. Different adsorption models, including the Freundlich, Tempkin, and Langmuir isotherms were assessed, and the best fit was found to be the Langmuir isotherm [41]:

$$\frac{C}{\theta} = \frac{1}{K_{\text{ads}}} + C \quad (8)$$

where C represents the concentration of HPP, K_{ads} delegates the equilibrium adsorption constant, θ means the degree of surface coverage, and the θ values were obtained from Table 2.

As shown in Figure 5, a straight line of C versus C/θ is found with the R^2 value close to 1, indicating that the fitting result is reliable. Moreover, the Gibbs free energy (ΔG_{ads}^0) can be described by the following equation [42]:

$$\Delta G_{\text{ads}}^0 = -RT \ln(55.5K_{\text{ads}}) \quad (9)$$

where 55.5 is the concentration of water molecules in the solution, T is the temperature, and R stands for the universal gas constant. The calculated value of ΔG_{ads}^0 is -25.692 kJ/mol , which is between -40 and -20 kJ/mol , indicating that the adsorption of inhibitors at the steel/solution interface is a spontaneous process, which belongs to the mixed chemisorption and physisorption process [43].

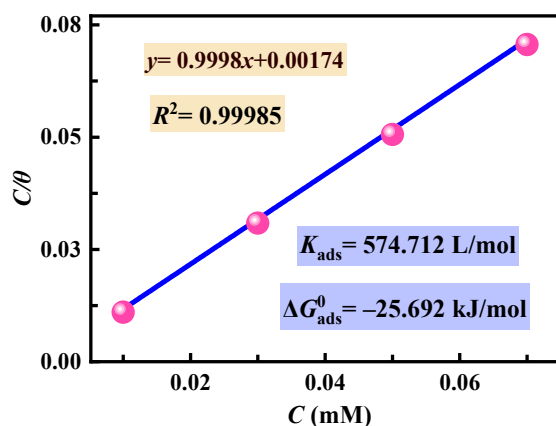


Figure 5. Langmuir adsorption isotherm model of HPP on mild steel surface in 1 M HCl solution.

3.4. SEM-EDS Analysis

We observed the surface morphology of mild steel by SEM after immersing it in the test solution for 6 h. As given in Figure 6a, the polished steel surface was smooth and clean. The surface of mild steel in blank condition was very rough and severely corroded, forming corrosion products such as chloride and oxide, which accumulate on the metal substrate (Figure 6b). As a result of adding HPP inhibitor to the corrosive solution, the surface of mild steel was smoother than it had been before (Figure 6c). This phenomenon was further verified by EDS mapping and point analysis (Figure 6d–i). Br and P elements were observed in the inhibited solution, while the composition of O element was significantly lower than in those without corrosion inhibitor. According to this observation, we can confirm the HPP molecules have been adsorbed onto the surface of the steel.

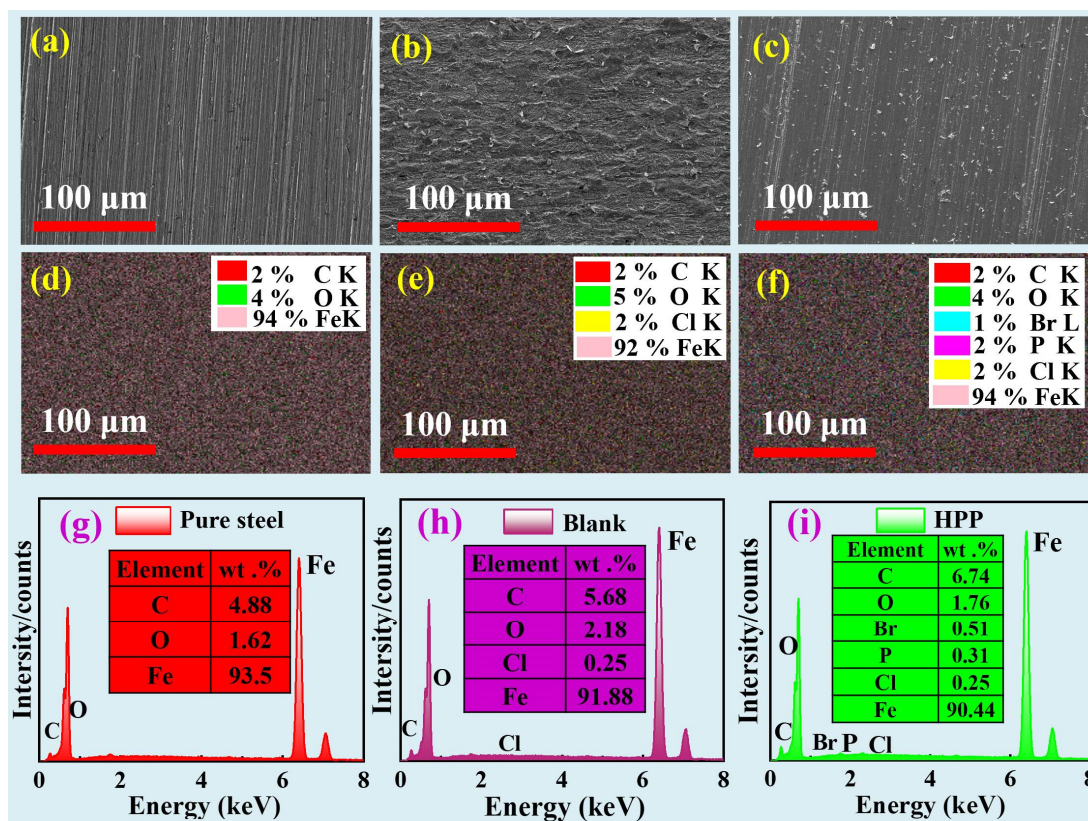


Figure 6. SEM-EDS results of mild steel at different tested conditions: (a,d,g) freshly polished mild steel, (b,e,h) in blank HCl solution, (c,f,i) with 0.07 mM HPP inhibitor.

3.5. UV-Visible Spectroscopy Study

As shown in Figure 7a, the peaks of 204 nm and 250 nm were observed when the mild steel was soaked in blank HCl solution for 6 h, which might be caused by the reaction of Fe with HCl while producing anionic chloride [44]. Additionally, the inhibitor-containing absorption band exhibits the peaks of 231 nm and 274 nm, demonstrating the π - π^* electron transition with charge transfer characteristics has taken place (Figure 7b). The change of absorption band positions indicated that HPP and Fe^{2+} may form a complex in acidic solution [45].

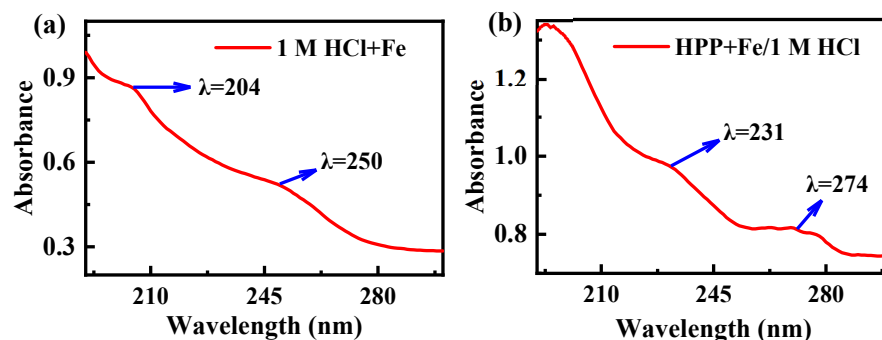


Figure 7. UV-visible spectra of mild steel immersed in (a) blank solution and (b) 1 M HCl solution with 0.07 mM HPP.

3.6. Computational Perspectives

To evaluate the relationship between HPP molecular structure and inhibitory performance, a quantum chemical computation was performed. Figure 8 depicts the optimized molecular structure of HPP, its highest occupied molecular orbital (HOMO), and lowest unoccupied molecular orbital (LUMO) densities, as well as the molecular electrostatic potential (ESP) map. A closer look at the distributions shows that most of the HOMOs and LUMOs are located around the triphenyl group. HOMO and LUMO densities relate to portions of a molecule that might possibly contribute to electron-donating and electron-accepting abilities, respectively [46]. The triphenyl moiety is richer in electrons thanks to its phenyl rings. When these rings interact with steel surfaces, their reactive sites act as adsorption centers.

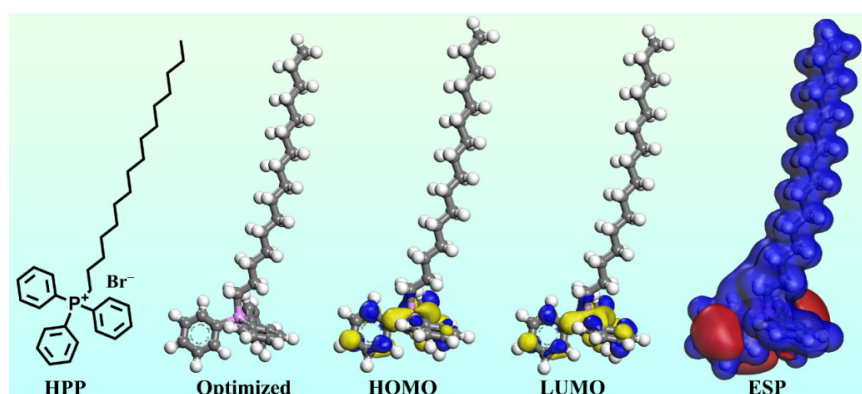


Figure 8. Optimized molecular structure, HOMO, LUMO, and molecular electrostatic potential of HPP inhibitor.

In recent years, MD simulations have become a standard tool alongside experiments to understand the anti-corrosion mechanism at an atomic scale, which can bring valuable information to interpret experimental data. Therefore, it is sometimes referred to as “computational microscopy” because of the ability to see like through a microscope the interactions between molecules and metal substrate. Herein, we performed MD simulations

with varying numbers of HPP molecules on Fe(110) substrate in aqueous environment. As can be seen from Figure 9, the polar triphenyl groups and bromide ions are tightly attached to the metal surface, while the hydrophobic alkyl chains are tipsily placed in aqueous solutions. Adsorption energy (E_{ads}) was determined using the following equation in order to measure the strength of the inhibitor adsorbed onto the metal surface [47]:

$$E_{\text{ads}} = E_{\text{total}} - (E_{\text{surf+solu}} + E_{\text{inh+solu}}) + E_{\text{solu}} \quad (10)$$

wherein, E_{total} means the total potential energy of the system, which include metal crystal, the adsorbed inhibitor molecule as well as medium solution; $E_{\text{surf+solu}}$ represents the total energy of metal surface and solution without the inhibitor; $E_{\text{inh+solu}}$ stands for the total energy of the inhibitor and solution; and E_{solu} represents the potential energy of the solvent molecules. It is commonly accepted that a larger adsorption strength between an inhibitor molecule and metal surface is indicated by a more negative value of E_{ads} [48]. When the number of HPP molecules is 1, 2, 3, and 4, the corresponding adsorption energies are -345.2 , -655.5 , -994.1 , and -1347.3 kcal/mol, respectively. These negative values indicate that the adsorptive system is stable and spontaneous adsorption can occur, which confirms the experimental finding that the corrosion inhibition efficiency increases with increasing inhibitor concentration within a certain range.

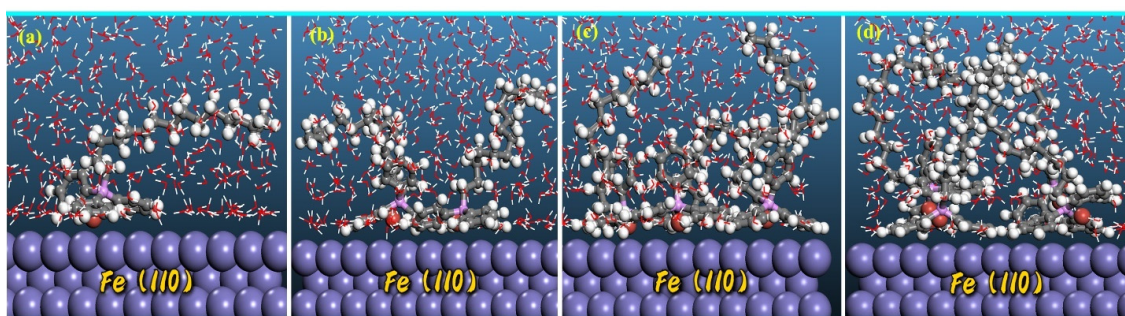


Figure 9. The most stable configurations for the adsorption of different numbers of HPP molecules on Fe(110) surface in acidic medium. (a) one, (b) two, (c) three, and (d) four.

3.7. Analysis of Anticorrosive Mechanism

A clear explanation of HPP inhibitor's anti-corrosion mechanism in 1 M HCl solution is provided in this section. As shown in Figure 10, below is a description of the anodic dissolution process of steel [49]:

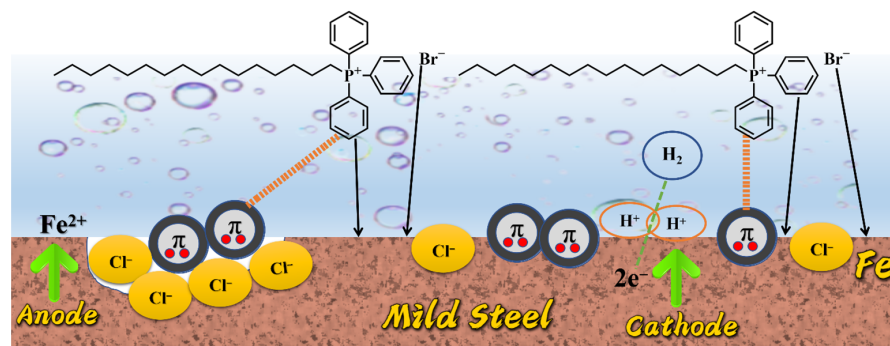


Figure 10. Adsorption mechanism of HPP on the surface of mild steel in acidic medium.

The electrons flowed to the cathode where hydrogen evolution reaction occurred [50]:



Earlier in this paper, we speculated that adding HPP to HCl solution would decrease corrosion rates, since HPP formed a barrier film on the steel surface through the adsorption of functional groups. Langmuir adsorption and MD simulations results showed that the hydrophilic part was spontaneously moved to the steel surface during the adsorption process. However, most of the hydrophobic tail was placed in the solution, resulting in the physisorption of the molecules. On the other hand, as a surfactant, HPP possesses an excess of bromine ions, which can accumulate on the steel surface to influence the inhibition process, resulting in a negatively charged metal surface. Afterwards, the positively charged HPP cation was electrostatically attracted to the negatively charged steel surface. Moreover, iron atoms on the steel surface would generate $3d$ empty orbitals, while electrons on HPP could be transferred to Fe orbitals for chemisorption. Therefore, physisorption and chemisorption occurred simultaneously in the adsorption process due to the *self-synergistic inhibition effect*, and a self-assembled barrier film was formed to mitigate the corrosion of mild steel.

4. Conclusions

Overall, HPP exhibited an excellent corrosion inhibition performance on mild steel in 1 M HCl solution due to the adsorption effect. The R_{ct} value and inhibition efficiency increased with the increase of corrosion inhibitor concentration at 298 K, and the inhibition efficiency was up to 99.1% in 0.07 mM HPP. PDP analysis showed that with the increase in HPP, the initial potential became more negative, β_a and β_c were shifted, which proved that the reaction was a complex of physical (electrostatic interaction) and chemical adsorption. SEM-EDX and UV-visible spectroscopy analysis revealed the formation of self-assembly HPP layer on the metal surface. Furthermore, we deduced that the electron donor and acceptor characteristics play a key role in the inhibition process, and the corrosion inhibition performance is further enhanced by the *self-synergistic inhibition effect* of the ionic liquid itself.

Author Contributions: Investigation, Y.H. and L.G.; Supervision, L.G. and W.S.; Writing—original draft, Y.H. and L.G.; Visualization, Y.W. and F.A.; Software, L.G. and F.A.; Data curation, Y.H., R.M., X.Z. and Y.W.; Project administration, L.G.; Funding acquisition, L.G. and R.M.; Writing—review and editing, Y.L. and W.S. All authors have read and agreed to the published version of the manuscript.

Funding: Riadh Marzouki extends his appreciation to the Deanship of Scientific Research at King Khalid University for funding this work through general research project under grant number (No. G.R.P. 182/43). This work is also supported by the Foundation of the Department of Science and Technology of the Guizhou province (No. QKHPTRC[2021]5643), the National Natural Science Foundation of China (No. 22262030, 22062022, 52074232), the China Postdoctoral Science Foundation (No. 2022M710117), and the Foundation of the Department of Education of the Guizhou province (No. QJJ[2022]003, QJHKY[2020]067).

Institutional Review Board Statement: Not applicable.

Informed Consent Statement: Not applicable.

Data Availability Statement: Data is contained within the article.

Conflicts of Interest: The authors declare no conflict of interest.

References

1. Abd El-Lateef, H.M. Experimental and computational investigation on the corrosion inhibition characteristics of mild steel by some novel synthesized imines in hydrochloric acid solutions. *Corros. Sci.* **2015**, *92*, 104–117. [[CrossRef](#)]
2. Slepski, P.; Gerengi, H.; Jazdzewska, A.; Orlikowski, J.; Darowicki, K. Simultaneous impedance and volumetric studies and additionally potentiodynamic polarization measurements of molasses as a carbon steel corrosion inhibitor in 1M hydrochloric acid solution. *Constr. Build. Mater.* **2014**, *52*, 482–487. [[CrossRef](#)]

3. Li, X.; Zhang, D.; Liu, Z.; Li, Z.; Du, C.; Dong, C. Materials science: Share corrosion data. *Nature* **2015**, *527*, 441–442. [[CrossRef](#)]
4. Cook, A.; Frankel, G.; Davenport, A.; Hughes, T.; Gibbon, S.; Williams, D.; Bluhm, H.; Maurice, V.; Lyth, S.; Marcus, P.; et al. Corrosion control: General discussion. *Faraday Discuss.* **2015**, *180*, 543–576. [[CrossRef](#)]
5. Sharma, S.; Kumar, A. Recent advances in metallic corrosion inhibition: A review. *J. Mol. Liq.* **2021**, *322*, 114862. [[CrossRef](#)]
6. Aslam, R.; Serdaroglu, G.; Zehra, S.; Kumar Verma, D.; Aslam, J.; Guo, L.; Verma, C.; Ebenso, E.E.; Quraishi, M.A. Corrosion inhibition of steel using different families of organic compounds: Past and present progress. *J. Mol. Liq.* **2022**, *348*, 118373. [[CrossRef](#)]
7. Verma, C.; Ebenso, E.E.; Quraishi, M.A.; Hussain, C.M. Recent developments in sustainable corrosion inhibitors: Design, performance and industrial scale applications. *Mater. Adv.* **2021**, *2*, 3806–3850. [[CrossRef](#)]
8. Chauhan, D.S.; Quraishi, M.A.; Sorour, A.A.; Verma, C. A review on corrosion inhibitors for high-pressure supercritical CO₂ environment: Challenges and opportunities. *J. Pet. Sci. Eng.* **2022**, *215*, 110695. [[CrossRef](#)]
9. Zhuang, W.; Wang, X.; Zhu, W.; Zhang, Y.; Sun, D.; Zhang, R.; Wu, C. Imidazoline gemini surfactants as corrosion inhibitors for carbon steel X70 in NaCl solution. *ACS Omega* **2021**, *6*, 5653–5660. [[CrossRef](#)]
10. Amendola, R.; Acharjee, A. Microbiologically influenced corrosion of copper and its alloys in anaerobic aqueous environments: A review. *Front. Microbiol.* **2022**, *13*, 806688. [[CrossRef](#)]
11. Han, P.; Chen, C.; Li, W.; Yu, H.; Xu, Y.; Ma, L.; Zheng, Y. Synergistic effect of mixing cationic and nonionic surfactants on corrosion inhibition of mild steel in HCl: Experimental and theoretical investigations. *J. Colloid Interface Sci.* **2018**, *516*, 398–406. [[CrossRef](#)]
12. Kobzar, Y.L.; Fatyeyeva, K. Ionic liquids as green and sustainable steel corrosion inhibitors: Recent developments. *Chem. Eng. J.* **2021**, *425*, 131480. [[CrossRef](#)]
13. Ardakani, E.K.; Kowsari, E.; Ehsani, A.; Ramakrishna, S. Performance of all ionic liquids as the eco-friendly and sustainable compounds in inhibiting corrosion in various media: A comprehensive review. *Microchem. J.* **2021**, *165*, 106049. [[CrossRef](#)]
14. Greer, A.J.; Jacquemin, J.; Hardacre, C. Industrial applications of ionic liquids. *Molecules* **2020**, *25*, 5207. [[CrossRef](#)]
15. El Hajjaji, F.; Ech-chihbi, E.; Salim, R.; Titi, A.; Messali, M.; El Ibrahim, B.; Kaya, S.; Taleb, M. A detailed electronic-scale DFT modeling/MD simulation, electrochemical and surface morphological explorations of imidazolium-based ionic liquids as sustainable and non-toxic corrosion inhibitors for mild steel in 1 M HCl. *Mater. Sci. Eng. B* **2023**, *289*, 116232. [[CrossRef](#)]
16. Liu, P.; Dai, S.; Lan, J.; Lu, H.; Wang, B.; Zhu, Y. Corrosion inhibition mechanism of imidazole ionic liquids with high temperature in 20% HCl solution. *J. Mol. Model.* **2022**, *29*, 29. [[CrossRef](#)]
17. Zheng, X.W.; Zhang, S.T.; Li, W.P.; Yin, L.L.; He, J.H.; Wu, J.F. Investigation of 1-butyl-3-methyl-1H-benzimidazolium iodide as inhibitor for mild steel in sulfuric acid solution. *Corros. Sci.* **2014**, *80*, 383–392. [[CrossRef](#)]
18. Meunier, M.; Robertson, S. Materials studio 20th anniversary. *Mol. Simul.* **2021**, *47*, 537–539. [[CrossRef](#)]
19. Huang, L.; Wang, Z.-M.; Wang, S.-S.; Wang, Y.-H.; Li, H.-J.; Wu, Y.-C. Environmentally benign cinchonain IIa from *Uncaria laevigata* for corrosion inhibition of Q235 steel in HCl corrosive medium: Experimental and theoretical investigation. *Environ. Res.* **2022**, *215*, 114376. [[CrossRef](#)]
20. Li, E.; Li, Y.; Liu, S.; Yao, P. Choline amino acid ionic liquids as green corrosion inhibitors of mild steel in acidic medium. *Colloid. Surface A* **2023**, *657*, 130541. [[CrossRef](#)]
21. Ahmad, Z.U.; Chao, B.; Konggidinata, M.I.; Lian, Q.; Zappi, M.E.; Gang, D.D. Molecular simulation and experimental validation of resorcinol adsorption on ordered mesoporous carbon (OMC). *J. Hazard. Mater.* **2018**, *354*, 258–265. [[CrossRef](#)] [[PubMed](#)]
22. Guo, L.; Qi, C.; Zheng, X.; Zhang, R.; Shen, X.; Kaya, S. Toward understanding the adsorption mechanism of large size organic corrosion inhibitors on an Fe(110) surface using the DFTB method. *RSC Adv.* **2017**, *7*, 29042–29050. [[CrossRef](#)]
23. Sun, H.; Ren, P.; Fried, J.R. The COMPASS force field: Parameterization and validation for phosphazenes. *Comput. Theor. Polym. Sci.* **1998**, *8*, 229–246. [[CrossRef](#)]
24. Abu-Rayyan, A.; Al Jahdaly, B.A.; AlSalem, H.S.; Alhadhrami, N.A.; Hajri, A.K.; Bukhari, A.A.H.; Waly, M.M.; Salem, A.M. A study of the synthesis and characterization of new acrylamide derivatives for use as corrosion inhibitors in nitric acid solutions of copper. *Nanomaterials* **2022**, *12*, 3685. [[CrossRef](#)] [[PubMed](#)]
25. McCafferty, E. Validation of corrosion rates measured by the Tafel extrapolation method. *Corros. Sci.* **2005**, *47*, 3202–3215. [[CrossRef](#)]
26. Nwankwo, H.U.; Ateba, C.N.; Olasunkanmi, L.O.; Adegunle, A.S.; Isabirye, D.A.; Onwudiwe, D.C.; Ebenso, E.E. Synthesis, characterization, antimicrobial studies and corrosion inhibition potential of 1,8-dimethyl-1,3,6,8,10,13-hexaazacyclotetradecane: Experimental and quantum chemical studies. *Materials* **2016**, *9*, 107. [[CrossRef](#)]
27. Betti, N.; Al-Amiery, A.A.; Al-Azzawi, W.K. Experimental and quantum chemical investigations on the anticorrosion efficiency of a nicotinehydrazide derivative for mild steel in HCl. *Molecules* **2022**, *27*, 6254. [[CrossRef](#)]
28. Singh, P.; Quraishi, M.A. Corrosion inhibition of mild steel using Novel Bis Schiff's Bases as corrosion inhibitors: Electrochemical and surface measurement. *Measurement* **2016**, *86*, 114–124. [[CrossRef](#)]
29. Zhang, W.; Zhang, Y.; Li, B.; Guo, H.; Dou, X.; Lu, K.; Feng, Y. High-performance corrosion resistance of chemically-reinforced chitosan as ecofriendly inhibitor for mild steel. *Bioelectrochemistry* **2023**, *150*, 108330. [[CrossRef](#)]
30. Laadam, G.; Benhiba, F.; El Faydy, M.; Titi, A.; Al-Gorair, A.S.; Alshareef, M.; Hawsawi, H.; Touzani, R.; Warad, I.; Bellaouchou, A.; et al. Anti-corrosion performance of novel pyrazole derivative for carbon steel corrosion in 1 M HCl: Computational and experimental studies. *Inorg. Chem. Commun.* **2022**, *145*, 109963. [[CrossRef](#)]

31. Mahfoud, H.; Rouag, N.; Boudiba, S.; Benahmed, M.; Morakchi, K.; Akkal, S. Mathematical and electrochemical investigation of *Lamium flexuosum* extract as effective corrosion inhibitor for CS in acidic solution using multidimensional minimization program system. *Arab. J. Sci. Eng.* **2022**, *47*, 6605–6616. [[CrossRef](#)]
32. Brug, G.J.; Vandeneeden, A.L.G.; Sluytersrehabach, M.; Sluyters, J.H. The analysis of electrode impedances complicated by the presence of a constant phase element. *J. Electroanal. Chem.* **1984**, *176*, 275–295. [[CrossRef](#)]
33. El-Haitout, B.; Hejjaj, C.; Lgaz, H.; Al-Hadeethi, M.R.; Ali, O.M.; Lee, H.S.; Ali, I.H.; Salghi, R. Superior long-term corrosion inhibition of N80 steel by new eco-friendly hydrazone-based compounds in a simulated oil well acidizing environment: Establishing the mechanism at the molecular level. *Langmuir* **2022**, *38*, 15937–15949. [[CrossRef](#)]
34. El Aatiaoui, A.; Daoudi, W.; El Boutaybi, A.; Guo, L.; Benchat, N.-E.; Aouinti, A.; Oussaid, A.; Loutou, M. Synthesis and anticorrosive activity of two new imidazo[1, 2-a]pyridine Schiff bases. *J. Mol. Liq.* **2022**, *350*, 118458. [[CrossRef](#)]
35. Guo, L.; Zhu, M.; He, Z.; Zhang, R.; Kaya, S.; Lin, Y.; Saji, V.S. One-pot hydrothermal synthesized nitrogen and sulfur codoped carbon dots for acid corrosion inhibition of Q235 steel. *Langmuir* **2022**, *38*, 3984–3992. [[CrossRef](#)]
36. Hu, K.; Zhuang, J.; Ding, J.; Ma, Z.; Wang, F.; Zeng, X. Influence of biomacromolecule DNA corrosion inhibitor on carbon steel. *Corros. Sci.* **2017**, *125*, 68–76. [[CrossRef](#)]
37. Huang, L.; Wang, S.S.; Li, H.J.; Wang, J.Y.; Li, Z.G.; Wu, Y.C. Highly effective Q235 steel corrosion inhibition in 1 M HCl solution by novel green strictosamide from *Uncaria laevigata*: Experimental and theoretical approaches. *J. Environ. Chem. Eng.* **2022**, *10*, 107581. [[CrossRef](#)]
38. Conway, B.E.; Bockris, J.O.M.; Ammar, I.A. The dielectric constant of the solution in the diffuse and Helmholtz double layers at a charged interface in aqueous solution. *Trans. Faraday Soc.* **1951**, *47*, 756–766. [[CrossRef](#)]
39. Zhu, M.; He, Z.; Guo, L.; Zhang, R.; Anadebe, V.C.; Obot, I.B.; Zheng, X. Corrosion inhibition of eco-friendly nitrogen-doped carbon dots for carbon steel in acidic media: Performance and mechanism investigation. *J. Mol. Liq.* **2021**, *342*, 117583. [[CrossRef](#)]
40. Jalab, R.; Saad, M.A.; Sliem, M.H.; Abdullah, A.M.; Hussein, I.A. An eco-friendly quaternary ammonium salt as a corrosion inhibitor for carbon steel in 5 M HCl solution: Theoretical and experimental investigation. *Molecules* **2022**, *27*, 6414. [[CrossRef](#)]
41. Mittal, A.; Kurup, L.; Mittal, J. Freundlich and Langmuir adsorption isotherms and kinetics for the removal of Tartrazine from aqueous solutions using hen feathers. *J. Hazard. Mater.* **2007**, *146*, 243–248. [[CrossRef](#)] [[PubMed](#)]
42. Mohamed, A.; Martin, U.; Bastidas, D.M. Adsorption and surface analysis of sodium phosphate corrosion inhibitor on carbon steel in simulated concrete pore solution. *Materials* **2022**, *15*, 7429. [[CrossRef](#)] [[PubMed](#)]
43. Kannan, P.; Rajeev, R.; Varghese, A.; Rajendran, N. Surface adsorption and anticorrosive behavior of benzimidazolium inhibitor in acid medium for carbon steel corrosion. *J. Appl. Electrochem.* **2022**, *52*, 1659–1674. [[CrossRef](#)]
44. Costa, M.; Carvalho, A.; Uryga, A.; Paiva, A. Solvent extraction of iron(III) from hydrochloric acid solutions using N,N'-Dimethyl-N,N'-diphenylmalonamide and N,N'-Dimethyl-N,N'-diphenyltetradecylmalonamide. *Solvent Extr. Ion Exch.* **2003**, *21*, 653–686. [[CrossRef](#)]
45. Rbaa, M.; Benhiba, F.; Obot, I.B.; Oudda, H.; Warad, I.; Lakhrissi, B.; Zarrouk, A. Two new 8-hydroxyquinoline derivatives as an efficient corrosion inhibitors for mild steel in hydrochloric acid: Synthesis, electrochemical, surface morphological, UV-visible and theoretical studies. *J. Mol. Liq.* **2019**, *276*, 120–133. [[CrossRef](#)]
46. Serin, S. DFT-based computations on some structurally related N-substituted piperazines. *J. Indian Chem. Soc.* **2022**, *99*, 100766. [[CrossRef](#)]
47. Qiang, Y.; Guo, L.; Li, H.; Lan, X. Fabrication of environmentally friendly Losartan potassium film for corrosion inhibition of mild steel in HCl medium. *Chem. Eng. J.* **2021**, *406*, 126863. [[CrossRef](#)]
48. Meng, S.; Liu, Z.; Zhao, X.; Fan, B.; Liu, H.; Guo, M.; Hao, H. Efficient corrosion inhibition by sugarcane purple rind extract for carbon steel in HCl solution: Mechanism analyses by experimental and in silico insights. *RSC Adv.* **2021**, *11*, 31693–31711. [[CrossRef](#)]
49. Guo, L.; Zhu, S.; Zhang, S.; He, Q.; Li, W. Theoretical studies of three triazole derivatives as corrosion inhibitors for mild steel in acidic medium. *Corros. Sci.* **2014**, *87*, 366–375. [[CrossRef](#)]
50. Shahsavari, M.; Imani, A.; Asselin, E. Pomegranate arils extract as a green corrosion inhibitor for mild steel: Effect of concentration and temperature in hydrochloric acid. *Mater. Res. Express* **2022**, *9*, 116517. [[CrossRef](#)]

Disclaimer/Publisher's Note: The statements, opinions and data contained in all publications are solely those of the individual author(s) and contributor(s) and not of MDPI and/or the editor(s). MDPI and/or the editor(s) disclaim responsibility for any injury to people or property resulting from any ideas, methods, instructions or products referred to in the content.